J MATER RES TECHNOL. 2020;9(3):3699–3709

Available online at www.sciencedirect.com

jmr&t Journal of Materials Research and Technology

www.jmrt.com.br

Original Article

Impact of magnetic field on boundary-layer flow of Sisko liquid comprising nanomaterials migration through radially shrinking/stretching surface with zero mass flux

Umair Khan[a], *A. Zaib*[b,*], *Zahir Shah*[c], *Dumitru Baleanu*[d,e,f], *El-Sayed M. Sherif*[g,h,i]

[a] *Department of Mathematics and Social Sciences, Sukkur IBA University, Sukkur 65200, Sindh, Pakistan*
[b] *Department of Mathematical Sciences, Federal Urdu University of Arts, Science & Technology, Gulshan-e-Iqbal, Karachi 75300, Pakistan*
[c] *Center of Excellence in Theoretical and Computational Science (TaCS-CoE), SCL 802 Fixed Point Laboratory, Science Laboratory Building, King Mongkut's University of Technology Thonburi (KMUTT), 126 Pracha-Uthit Road, Bang Mod, Thrung Khru, Bangkok 10140, Thailand*
[d] *Department of Mathematics, Cankaya University, Ankara, Turkey*
[e] *Institute of Space Sciences, 077125 Magurele, Romania*
[f] *Department of Medical Research, China Medical University Hospital, China Medical University, Taichung, Taiwan*
[g] *Research Chair for Tribology, Surface, and Interface Sciences (TSIS), Department of Physics and Astronomy, College of Science, King Saud University, P.O. Box 2455, Riyadh 11451, Saudi Arabia*
[h] *Center of Excellence for Research in Engineering Materials (CEREM), King Saud University, P.O. Box 800, Al-Riyadh 11421, Saudi Arabia*
[i] *Electrochemistry and Corrosion Laboratory, Department of Physical Chemistry, National Research Centre, El-Buhouth St., Dokki, 12622 Cairo, Egypt*

ARTICLE INFO

Article history:
Received 14 January 2020
Accepted 31 January 2020
Available online 10 February 2020

Keywords:
Nanofluids
Magnetic-Sisko fluid
Convective heat transfer
Zero mass flux
Radially shrinking/stretching surface

ABSTRACT

In the recent past, many claims on thermo-physical characteristics of nanofluids in different flow regimes, especially laminar flow regime have been comprised in literature. Keeping these in mind, the focus of the current review is to study the physical aspects of laminar two-dimensional flow of magnetic-Sisko fluid where nanoparticles are present. In addition, the mass and the heat transfer features through convective boundary and zero mass flux conditions have been examined. This paper is probably the first contribution concerning the multiple solutions for axi-symmetric flow of Sisko nanofluids owing to a radially shrinking surface. The physical situation is modelled with the aid of mass, momentum and energy conservation equations. This investigation employs the non-dimensional variables to transmute the conserving PDE's to a system of ODE's. In the numerical study, a collocated numerical technique, namely, bvp4c based on finite difference technique is utilized to obtain the results of the aforementioned problem. This scheme allows us to acquire the multiple solutions (lower and upper) for various specific values of shrinking and suction constraint. The outcomes from this review exhibit that the suction parameter accelerates the local skin

* *Corresponding author.*
E-mail: aurangzaib@fuuast.edu.pk (A. Zaib).
https://doi.org/10.1016/j.jmrt.2020.01.107

friction in the phenomenon of the first solution while a repeal trend is watched for the second solution. It is further visualized that the presence of a high magnetic field shrinks the liquid velocity. In addition, the Sisko constraint decelerates the skin friction and the Nusselt number in the first solution and accelerated in the second solution. Finally, the results of a current study established a superb correlation with existing data for selected parameter values.

1. Introduction

At the moment, the world is encountering with a major issue of poor thermal conductivity of functioning liquids which impedes great solidity and efficiency of thermal production in heat interchanges. Mostly the usual working fluids are ethanol, water, acetone and the mixture of ethylene-glycol. In addition, to this problem the researchers, scientists and engineers have displayed their key rule in advancement of thermal features of energy transmission liquids and the transfer of heat performance of the industrial appliances. In general, an innovative technique of enhancing the poor thermal conductivities is mainly categories in two ways: active methods, in which some external forces are required, for instance, an electrical field and the second one are the passive method, in which some specific surface geometries or fluid additives are necessary. In accordance with the poor thermal conductivity of the most widely recognized liquids and keeping in mind the much better thermal conductivity of solids, we add some solid particles into an ordinary liquid to improve its heat transfer capabilities. Therefore, several experimental efforts have proven that an efficient way of improving low quality of thermal conductivities is to suspend solid flecks in the functioning fluids. Different sorts of powders, for example, carbon-based nanostructures, metallic and non-metallic can be added with the functioning to form liquid mixtures. This has shown great improvement in the presence of thermal conductivities of base fluids [1,2]. Subsequently, enormous scientists endeavored to append present kind of nanostructures within the base liquids to form predominant heat transfer liquids.

As discussed before, utilizing nanoparticles greatly affects heat transfer rate in modern industrial applications. A great deal of study has been conducted on the particles of whole dimensions such as micro, nano and macro etc. On the other hand, due to some hindrance nano-second flecks have pulled in numerous considerations. Fairly the aforementioned particles are small in body and almost equal to the size of atoms of working liquid and comprehend highly stable suspensions. However, the division of such insulator particles whose capacity is lower than 100 nm in working fluids is termed as ñanofluids:. This word was first employed by Choi [3] in 1995. The implications of the given study employed nanoparticles to boost up the thermal conductivities of functioning fluids. He investigated more empirical work which mean more generic and computational studies in research works to know that how its boost up the thermal conductivity. Later, Eastman et al. [4] has exposed that, the thermal conductivities were used to raise the based nanofluid up to 60% under the addition of ethylene glycol and also combined with the base fluid with CuO nanoparticles of volume fraction 5%. Mostly the key and speedily implemented mechanism in the industrialist appliances are the Brownian and the thermophoresis phenomena in progress. Thus, Buongiorno [5] presented that this without source term model can foresee the nanoliquid coefficient of heat transfer, whereas the division influence is absolutely insignificant by cause of nanoparticle body. Hence, Buongiorno gave a different model to analyze the amazing transfer rate of heat growth in nanoliquids and thus obliterate out the negligibility of dispersion and homogeneous models. Afterward, Tiwari and Das [6] considered the flow of heat transfer characteristics of nanofluids in a problem of lid driven square cavity. In addition, Kuznetsov and Nield [7] utilized the model of Buongiorno to consider the influences of thermophoresis & Brownian in the presence of nanoscaled particles from a vertical surface under the assumption of free convective flow. After that, a numerous studies are presented to investigate the improvement of the transfer rate of heat features in flow of nanoliquids over distinct geometries, like, Rashidi et al. [8], Sheikholeslami et al. [9], Khan et al. [10], Rocha et al. [11] and Khan et al. [12], etc. In recent times, Ahmed et al. [13] explored the time dependent flow with the characteristic of heat transfer containing carbon nanotubes from a shrinking sheet with variable viscosity and obtained the numerical solution by utilizing Keller-box technique. Sheikholeslami [14] examined the influence of Lorentz force on ferroliquid under the treatment of entropy generation through porous media with exergy loss. The analysis of entropy generation on pressure driven flow comprising the water based aluminum oxide nanoliquid through porous medium with radiaitve electromagnetic field was explored by Ellahi et al. [15]. Sheikholeslami et al. [16] discussed the behavior of heat transfer in the presence of nanoliquid via PCM solidification by an enclosure through V shaped fins. Ellahi et al. [17] scrutinized the influence of entropy generation on electro-osmotic Couette-Poiseuille flow of power law liquid containing aluminum oxide particle with constant pressure gradient. Riaz et al. [18] discussed the influence of entropy generation of a Williamson liquid on the asymmetric peristaltic flow in the presence of convective condition. Sarafraz et al. [19] analyzed the impact of critical heat flux on the characteristic of heat transfer in pool boiling under the influence of iron oxide nano suspension and also visualized the bubble pattern with magnetic field. Ellahi et al. [20] investigated the slip influence in a two phase flow containing a nano size Hafnium materials. They examined the flow problem by considering the two distinct cases namely, particle phase and liquid phase.

In the recent few decades, the development in dissimilar fields of natural sciences and technologies has recommended

the scientists and researchers to spread their research towards the flow involving non-Newtonian liquids and the characteristics of heat transfer. It has been acknowledged that many fluids used in industry, biological processes and chemical engineering process do not hold the Newtonian law called it a non-Newtonian fluid. Various key industrialist liquids, including polymers, pulps, molten plastics, fossil fuel and food show non-Newtonian conduct. For this reason, a significant consideration has been dedicated to exploring the characteristics of power law liquids. The complication is based that not a single conserving equation demonstrated the gross features of such fluids called non-Newtonian is available. In research articles, most of models for non-Newtonian fluid specially concern simple models like the grade one, grade two or three and power-law [21,22]. In such manner, numerous methods have been designed to catch the rheology of power-law liquids, in which the shear stretch is power-law function of the strain rate. Among all non-Newtonian models, currently, numerous researchers have done lots of studies and made awesome achievements on the Sisko fluid model. Because of its wide applications in the chemical industry, Sisko model has much importance because it predicts the properties of numerous non-Newtonian liquids. This is a model for three-parametric which can be assumed as a generic of power-law and Newtonian model. The characteristics of shear thickening and shear thinning can be described by a Sisko model for a distinct range of power law index. The generalized Newtonian Sisko fluid model was first introduced by Sisko [23] in 1958. It was basically presented to measure higher shear rates in lubricating greases. A numerical investigation of an electrically conducting Sisko liquid in a symmetric or asymmetric channel for peristaltic flow had been presented by Wang et al. [24]. Later, Abelman et al. [25] explained the time-dependent flow of non-Newtonian Sisko liquid. They assumed that the flow is rotating and electrically conducting with the variable magnetic field. Furthermore, a mathematical formulation for the unidirectional flow of Sisko liquid in a cylindrical tube is presented by Khan et al. [26]. In this study cylindrical polar coordinates are employed to obtain the governing equations and their exact steady-state solutions are achieved. Very recently, lots of studies have been demonstrated by various authors the heat transfer and the flow characteristics of Sisko liquid due to different geometries [27–30].

The upgrading in industry and enhanced engineering expertise, the magnetohydrodynamic (MHD) flow of an electrical conducting nanofluid formed by the deformation of the wall on the surface are an active area of research and interest in modern processes of metallurgical and metal working. Applications of magnetic field to the flow of nanofluid has drawn great amount of ascension of various researchers owing to its overwhelming industrial and engineering applications. These types of fluid flows are more appropriate in the geothermal energy extraction, optical modulators, plasma confinement, tunable optical fiber filters, nuclear reactors, polymer industry, etc. Furthermore, Magnetic nanoliquids are colloidal suspensions comprising magnetizable nanomaterials, which seize the properties of magnets, liquid and thermal. They have distinct applications, for instance, in signal processing, optical communications, magneto optical tunable filter, tumor analysis & cancer therapy, etc. The majority of the physical characteristic of such liquids can be exposed through the unstable magnetic field. Siddappa and Abel made first effort to analyze the influence of magnetic field on flows of non-Newtonian liquids [31]. After that, MHD flow along with the transfer of heat characteristics nanoparticles past a porous stretched surface with slip conditions have been scrutinized by Ibrahim and Shankar [32]. In addition, Malvandi and Ganji [33] bestowed a theoretical review to study the fully developed flow along Al_2O_3-water nanofluid along convective heat transfer. They implemented the modified Buongiorno's model for the nanoliquid flow within a vertical micro-tube together with a uniform magnetic field. Sheikholeslami et al. [34] scrutinized the water based hydro magnetic CuO nanoliquid flow with heat transfer by deeming the impact of Lorentz forces. In this analysis, they observe an increment in heat transfer with a higher magnetic field. Recently, the Marangoni boundary-layer flow of nanofluids containing Copper and Titanium dioxide nanoparticles has been probed by Emad and Ebaid [35]. They found the exact solutions for the flow and temperature field via Laplace transform method. Very recently, too many investigations have been given to the influence of magnetic field in some other related works [36–38].

2. Objectives of this study

In view of the above discussion, we see that the existing literature provides sufficient guidance in the existence of nanoparticles with heat transfer and mass transfer to label the flow of Sisko fluids. A large bulk of the existing review addresses such issues using firstly, Sisko fluid flow past different stretching geometries and secondly, they obtained the single solutions for their flow field equations by means of different methods. However, there are certain physical situations in which we can utilize some numerical technique to establish the dual solutions for our flow problem. Most of the published work doesn't study such physical situation by considering Sisko fluid flow. Thus, the impacts of magnetic field on 2-D flow involving Sisko nanoliquid by considering Buongiorno model through a radially stretched/shrinking surface in the presence of convective boundary condition and zero mass flux condition is explored. The calculations of the present governing equations like, momentum, energy along with concentration have been constructed via a built in Matlab code bvp4c, which uses the finite difference scheme. Finally, the influences of numerous substantial parameters such as: material constraint for Sisko fluid, magnetic constraint, mass transfer constraint, stretching/shrinking parameter, thermophoresis and Brownian motion, Lewis & Prandtl number Pr on the Sisko nanoparticles flow, heat and mass transfer characteristics are investigated.

The contents of this paper are divided up as follows: The description of physical model is clearly prescribed in Section 2. In this section, the mathematical model for the 2-D incompressible flow of Sisko nanofluids with heat and mass transfers has been presented. In Section 3, the thermophysical quantities of engineering concern are clearly written in their dimensional form. A complete detailed description of the applied numerical scheme and code validation and also the results and graphs are scrutinized in Sections 5 and 6,

respectively. Finally, the main findings of the current study have been given in Section 7.

3. Problem formulation

We have considered an axi-symmetric steady flow of incompressible Sisko nanoliquids passed via radially shrinking sheet. In this model of nanofluids, we have included the influence of thermophoresis and Brownian motion. The cylindrical polar coordinates (r, z) are assumed in such manner that the $r-$ axis runs along the surface and the $z-$ axis is in the normal direction. The radially shrinking surface is laid down at $z = 0$ and it has a power- law velocity $u_w = cr^m$, where c and m are positive real numbers. Fig. 1 interprets a clear-cut scenario of this work which was driven to be computed. We explore into the impact of an external variable magnetic field $B(r) = B_0 r^{\frac{m-1}{2}}$ applied normal to the sheet. Further, the constant mass flux velocity $w = w_0$ is taken so that $w_0 > 0$ refers for suction while $w_0 < 0$ for injunction on the sheet along the $z-$ axis. The wall temperature T_w is the outcome of the convective heating phenomenon caused by the hot fluid means of temperature T_f which gives a coefficient of heat transfer h_f. The ambient fluid temperature is T_∞ as $(z \to \infty)$ such that $(T_f > T_\infty)$. Thus, the nanoparticles volume fraction of the surface of radially stretching sheet is kept at a constant value C_w.

The aforementioned boundary-layer region emphasizes the implication of Oberbeck-Boussinesq approximations & the standard conservation equations for the mingled mass and heat transfer analysis under consideration can be followed as:

$$\frac{\partial u}{\partial r} + \frac{\partial w}{\partial z} = -\frac{u}{r}, \tag{1}$$

$$u\frac{\partial u}{\partial r} + \frac{b}{\rho}\frac{\partial}{\partial z}\left(-\frac{\partial u}{\partial z}\right)^n + w\frac{\partial u}{\partial z} = \frac{a}{\rho}\left(\frac{\partial^2 u}{\partial z^2}\right) + \frac{\sigma B^2}{\rho}u, \tag{2}$$

$$(\rho c)_f\left(u\frac{\partial T}{\partial r} + w\frac{\partial T}{\partial z}\right) - (\rho c)_p\left(\frac{D_T}{T_\infty}\left(\frac{\partial T}{\partial z}\right)^2 + D_B\left(\frac{\partial C}{\partial z}\frac{\partial T}{\partial z}\right)\right) = k\frac{\partial^2 T}{\partial z^2}, \tag{3}$$

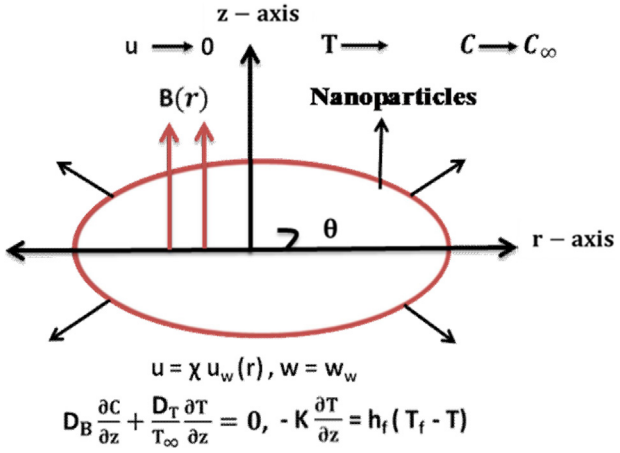

Fig. 1 – Physical diagram of the problem.

$$u\frac{\partial C}{\partial r} - \frac{D_T}{T_\infty}\frac{\partial^2 T}{\partial z^2} = D_B\frac{\partial^2 C}{\partial z^2} - w\frac{\partial C}{\partial z}. \tag{4}$$

The physical boundary conditions for the aforementioned fields are

$$\begin{aligned} &u = \chi u_w, w = w_w, -k\frac{\partial T}{\partial z} = h_f(T_f - T), \frac{D_T}{T_\infty}\frac{\partial T}{\partial z} \\ &+D_B\frac{\partial C}{\partial z} = 0 \text{ at } z = 0, \\ &u \to 0, T \to T_\infty, C \to C_\infty \text{ as } z \to \infty. \end{aligned} \tag{5}$$

We denote the components u and w in such a way that the corresponding velocity run along in $r-$ axis and $z-$ axis, respectively, σ, the electric conductivity, ρ, the fluid density, D_B, the coefficient of Brownian motion, D_T, the thermophoresis, k, the thermal conductivity, T, the liquid temperature, n, the power-law index and C, the concentration of nanoparticles. The boundary condition $\frac{D_T}{T_\infty}\frac{\partial T}{\partial z} + D_B\frac{\partial C}{\partial z} = 0$ at $z = 0$ in Eq. (5) exemplified the condition called mass flux condition of nanoparticles and which is vanished with consideration of thermophoresis proposed by Nield and Kuznetsov [7].

To facilitate the analysis, the following non-dimensional functions $f(\eta)$ and $\theta(\eta)$ along with the suitable parameter η are employed as:

$$\begin{aligned} &\eta = \frac{z}{r}Re_b^{\frac{1}{n+1}}, \psi = -u_w r^2 Re_b^{\frac{-1}{n+1}} f(\eta), \theta(\eta) = \frac{T_\infty - T}{T_\infty - T_w}, \\ &\phi(\eta) = \frac{C_\infty - C}{C_\infty - C_w}. \end{aligned} \tag{6}$$

The Stokes stream function $\psi(r, z)$ is such that $u = -\frac{1}{r}\frac{\partial \psi}{\partial z}$ and $w = \frac{1}{r}\frac{\partial \psi}{\partial r}$ which identically satisfy the continuity Eq. (1). The dimensional form of leading equations of liquid motion is followed:

$$f'''\left(A + n(-f'')^{n-1}\right) + \left(\frac{m(2n-1)+n+2}{n+1}\right)ff'' - M^2 f' - m(f')^2 = 0, \tag{7}$$

$$\frac{1}{Pr}\left(\theta'' + Nb\theta'\phi' + Nt(\theta')^2\right) + \left(\frac{m(2n-1)+n+2}{n+1}\right)f\theta' = 0, \tag{8}$$

$$\phi'' + \left(\frac{m(2n-1)+n+2}{n+1}\right)PrLef\phi' + \frac{Nt}{Nb}\theta'' = 0, \tag{9}$$

Together with transmuted boundary conditions:

$$\begin{aligned} &f(0) = S,\ \theta'(0) = -\gamma(1 - \theta(0)),\ f'(0) = \chi,\ Nt\theta'(0) + Nb\phi'(0) = 0, \\ &f'(\infty) \to 0,\ \phi(\infty) \to 0,\ \theta(\infty) \to 0. \end{aligned} \tag{10}$$

Prime ($'$) represents the differentiation with η. In addition, the important thermosical constraints signifying the dynamics of flow are the material constraint of the Sisko liquid A,

the magnetic constraint M, the mass transfer constraint S, the stretching & shrinking parameter χ, the thermophoresis parameter Nt, the Lewis number Le, the Brownian motion Nb and the Prandtl number Pr are expressed as

$$A=\frac{Re_b^{\frac{2}{n+1}}}{Re_a},\ M^2=\frac{\sigma B_0^2}{\rho u_w},\ S=\frac{w_w}{\left(\frac{m(2n-1)+n+2}{n+1}\right)u_w Re_b^{\frac{-1}{n+1}}},$$
$$Pr=\frac{ar^{m+1}}{\alpha_f}Re_b^{\frac{-2}{n+1}},\ Le=\frac{\alpha_f}{D_B},$$
$$Nb=\frac{(\rho c)_p D_B C_\infty}{(\rho c)_f \alpha_f},\ Nt=-\frac{(\rho c)_p D_T(T_\infty-T_f)}{(\rho c)_f \alpha_f T_\infty}. \tag{11}$$

where, $Re_a=\frac{\rho r u_w}{a}$ and $Re_b=\frac{\rho r^n u_w^{2-n}}{b}$ represents the local Reynolds numbers.

4. Parameters of physical concerns

From an engineering point of view, the substantial physical quantities are the friction factor C_{fr} in radial direction and the Nusselt number Nu_r.

4.1. Skin friction coefficient

The shear stress rate C_{fr} is delineated as

$$C_{fr}=\frac{2\tau_w}{\rho u_w^2},$$

where

$$\tau_w=a\left(\frac{\partial u}{\partial z}\right)-b\left(-\frac{\partial u}{\partial z}\right)^n\Big|_{z=0}, \tag{12}$$

Invoking Eq. (6), the reduced skin friction takes the form

$$\frac{1}{2}C_{fr}Re_b^{1/(n+1)}=Af''(0)-[-f''(0)]^n. \tag{13}$$

4.2. Local Nusselt number

The heat transfer rate Nu_r is classified as

$$Nu_r=\frac{xq_w}{k\left(T_f-T_\infty\right)},$$

where

$$q_w=-k\nabla T+h_p j_p, \tag{14}$$

and $q_m=\frac{j_p}{\rho_p}$ is the mass flux of the nanomaterial. Where

$$j_p=-\rho_p D_B\nabla C-\rho_p D_T\frac{\nabla T}{T},\ h_p=c_p T. \tag{15}$$

In perspective of using Eq. (14) in Eq. (15), we establish the dimensional form as follow:

$$Nu_r Re_b^{1/(n+1)}=-\theta'(0). \tag{16}$$

It is appealing to observe that due to modified condition $Nt\theta'(0)+Nb\phi'(0)=0$, the Sherwood number expression happened to identically zero specified by Kuznetsov and Nield [39].

5. Applied numerical method

In the present work, the governing equations for mass and analysis of heat transfer of an axi-symmetric flow of Sisko-nanoliquids through a radially shrinking sheet are mathematically modeled. These modeled equations are not linear in nature which is highly non-linear and it is not feasible to get their exact solutions. Thus, the simulations were performed for solving these non-linear differential Eqs. (7–9) with assisting boundary condition (10) via numerical technique based on a finite difference method called bvp4c routine. This technique is capable of handling first order initial value problems. To accomplish this, we assume the new variables

$$f=y_1, f'=y_2, f''=y_3, \theta=y_4, \theta'=y_5, \phi=y_6, \phi'=y_7, \tag{17}$$

Therefore, we get the following first-order system

$$\begin{pmatrix} y_1' \\ y_2' \\ y_3' \\ y_4' \\ y_5' \\ y_6' \\ y_7' \end{pmatrix}=\begin{pmatrix} y_2 \\ y_3 \\ \frac{M^2y_2+my_2^2-\left\{\frac{m(2n-1)+n+2}{n+1}\right\}y_1y_3}{A+n(-y_3)^{n-1}} \\ y_5 \\ -Nby_5y_7-Nty_5^2+Pr\left\{\frac{m(1-2n)-(n+2)}{n+1}\right\}y_1y_5 \\ PrLe\left\{\frac{m(1-2n)-(n+2)}{n+1}\right\}y_1y_7-\frac{Nb}{Nt}y_5' \end{pmatrix}, \tag{18}$$

and transformed initial conditions are

$$\begin{pmatrix} y_1(0) \\ y_2(0) \\ y_2(\infty) \\ y_5(0) \\ y_4(\infty) \\ y_7(0) \\ y_6(0) \end{pmatrix}=\begin{pmatrix} S \\ \chi \\ 0 \\ \gamma(y_4(0)-1) \\ 0 \\ -\frac{Nb}{Nt}y_5(0) \\ 0 \end{pmatrix}. \tag{19}$$

During this investigation, the nonlinear set of ordinary differential Eqs. (18 and 19) are tackled numerically by employing the Matlab function bvp4c. Considered as the problem may possess multiple solutions, therefore the said numerical scheme requires different initial guesses to fulfill the boundary conditions (19). The corresponding initial estimate for the first solution is relatively simple and easy to find. However, it is quite hard to find the initial guess for the lower branch solution owing to convergence problems. In order to conquer this trouble, we begin with some fixed values of physical parameters for which the solutions simpler to appear. At that point, we utilize the acquired outcomes and suppose it as an initial

Table 1 – A comparison of skin friction $\frac{1}{2}C_{fr}Re_b^{1/(n+1)}$ (first solution) for different values of M and A.

M	A	$\{n, m\} = \{0, 1\}$		$\{n, m\} = \{1, 3\}$	
		Khan et al. [41]	Present study	Khan et al. [41]	Present study
1.0	0.0	1.0000000	1.0000000	2.000000	2.000000
	0.5	2.000000	2.000000	2.449489	2.4494861
	1.0	2.414213	2.4142136	2.828427	2.8284274
	1.5	2.732050	2.7320540	3.162277	3.1622814
	2.0	3.000000	3.0000065	3.464101	3.4641183
2.0	0.0	1.0000000	1.0000000	2.645751	2.6457515
	0.5	2.581138	2.5811389	3.240370	3.2403705
	1.0	3.236067	3.2360679	3.741657	3.7416571
	1.5	3.738612	3.7385391	4.183300	4.1833000
	2.0	4.162277	4.1622819	4.582575	4.5825757

Table 2 – A comparison of skin friction $Re_b^{-1/(n+1)}Nu_r$ (first solution) for different values of Pr and γ.

Pr	γ	$\{n, m\} = \{0, 1\}$		$\{n, m\} = \{1, 3\}$	
		Khan et al. [41]	Present study	Khan et al. [41]	Present study
1.0	0.1	0.083367	0.08342479	0.091490	0.09149092
	0.2	0.142959	0.14312625	0.168632	0.16863275
	0.5	0.250312	0.25082570	0.341291	0.34129153
	1.0	0.333888	0.33480300	0.518121	0.51812226
2.0	0.1	0.089166	0.08916644	0.094278	0.09427889
	0.2	0.160900	0.16090154	0.178353	0.17835396
	0.5	0.311041	0.31104384	0.383607	0.38360797
	1.0	0.451465	0.45147118	0.622343	0.62234414

guess for the upcoming values of the constraints. It is known as a continuation method for boundary value problem [40]. In our computations, we have to consider the range of numerical integration (such as.$\eta_{\max} = 10.$) to be finite dimensions which is enough for the profiles to attain the wide field asymptotically at the boundary condition. The step size is taken as $\Delta\eta = 0.01$. The process is iteratively repeated until obligatory solutions with a satisfactory level of accuracy (i.e., up to 10^{-5}) to fulfill the criterion of convergence.

5.1. *Validation of solution methodology*

Validation to ensure correctness, uniformity and dependability of the numerical results are extremely significant in order to find a numerical solution of ODE's. To find out the accurate calculations through the bvp4c integration method in this article, a comparison of the $\frac{1}{2}C_{fr}Re_b^{1/(n+1)}$ and $Nu_rRe_b^{1/(n+1)}$ (for the upper branch solution) is assembled for limiting phenomenon (without the suction parameter) and for the stretching sheet ($\chi = 1$) with earlier reported work of Khan et al. [41]. These comparisons are shown through Tables 1 and 2. From these Tables, we noticed that our numerical outcomes are in good harmony with existing results. This comparison further ascertains the precision of the numerical solutions with obtaining HAM solutions.

6. Results and discussion

Here, the impacts of the physical constraints involved on characteristics of thermo-liquid in the regime of nanoliquid boundary layers are assessed. Therefore, the distributions are presented to see the influence parameters on A, M, S, χ, Nt, Nb, Le, Pr and its impacts are illustrated in terms of nanofluid velocity, concentration and temperature. For numerical examination, we set the following values of the emerging physical parameters $A = 2$, $M = 0.1$, $\chi = -1$, $S = 3$, $\mathrm{Pr} = 1.05$, $Nt = Nb = 0.5$, $m = 5$, $Le = 1$, $\gamma = 0.1$ and $n = 0.8$. Moreover, to delineate the flow dynamics, heat and mass transfers, the local skin friction coefficient, the local Nusselt number, the nanoparticles concentration, we sketched the Figs. 2–7 for distinctive values of pertinent constraints.

6.1. *Variations in skin and Nusselt number*

Fig. 2(a and b) emphasize the deviation of the skin factor $Af''(0) - [-f''(0)]^n$ and the heat transfer rate $-\theta'(0)$ at the wall verses shrinking parameter χ for distinct values of suction parameter S. We focus here to study the actuality of the dual solutions in case of shrinking sheet $\chi < 0$ for a certain parameter domain. These multiple solutions are also recognized as 1st solution (upper branch) and 2nd solution (lower branch). The first solution is represented by a solid line and the second solution is captured with a dotted line. Moreover, the studies reported by Miklavčič and Wang [42] and Feng et al. [43] mentioned that the multiple solutions occurred only for mass suction S. From our analysis, it is observed that we can acquire the solutions capability in a certain range for the stretched/shrinking parameter χ. In view of our numerical calculations, the situation for dual is identified that there exists a critical value $\chi_c < 0$ for which the behaviors of the dual solutions are same. This means that upper and lower branches join with each other at the critical point. However, the surface of the boundary layer split at $\chi = \chi_c$. It is depicted

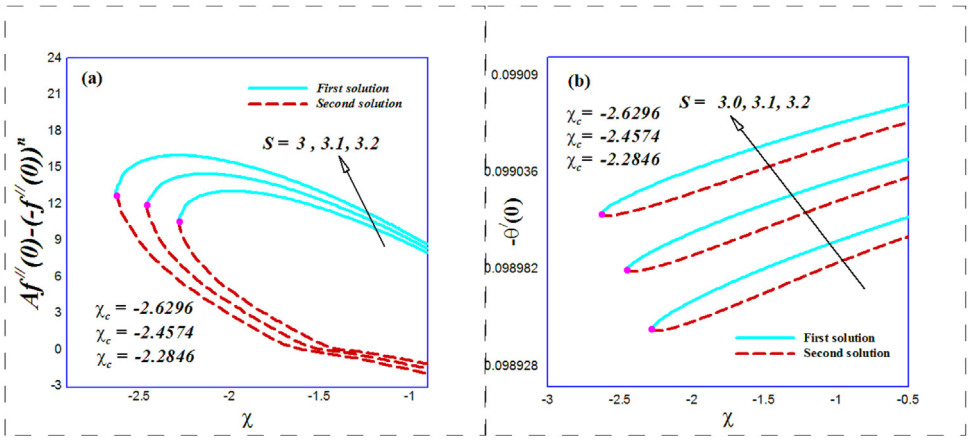

Fig. 2 – (a–b): Impact of S on (a) $Af''(0) - [-f''(0)]^n$, (b) $-\theta'(0)$ versus χ.

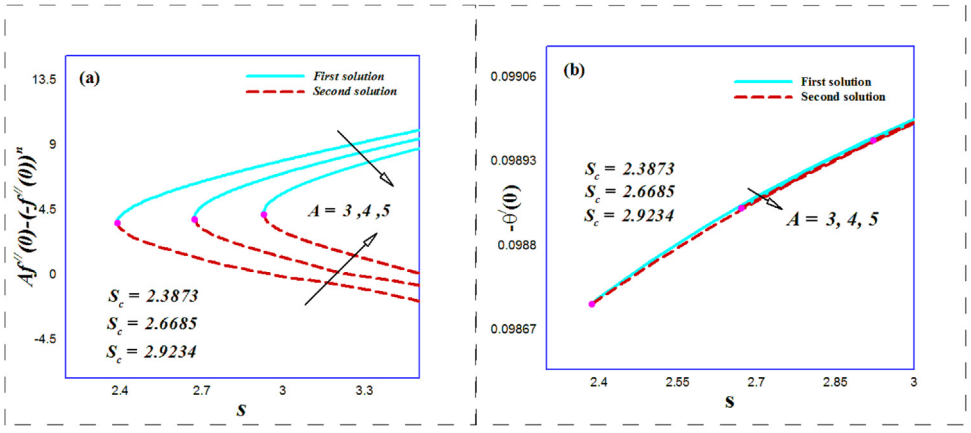

Fig. 3 – (a–b): Impact of A on (a) $Af''(0) - [-f''(0)]^n$, (b) $-\theta'(0)$ versus S.

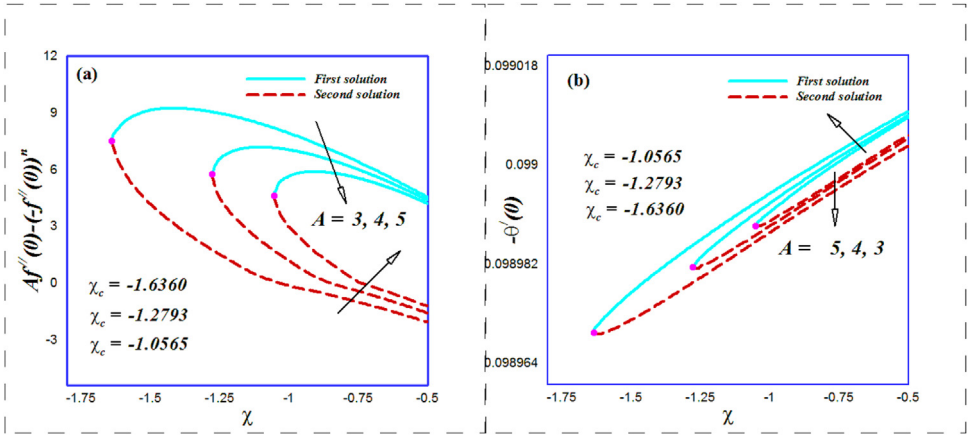

Fig. 4 – (a–b): Impact of A on (a) $Af''(0) - [-f''(0)]^n$, (b) $-\theta'(0)$ versus χ.

in Fig. 2(a,b) that the values of χ_c decline with augmenting of suction parameter for which it can be concluded that the existing domain of solution enhances with rising values of mass transfer parameter S. Moreover, an accelerating trend is perceived for the skin coefficient of the first solution, whilst depreciation for the second solution is noted with higher suction strength. In addition, the graph in Fig. 2(b) confirms the aforesaid condition on χ of existence of multiple solutions. It is observed from these graphs that the heat transfer rate augments for lower and upper branch solutions by raising the suction parameter. It is worth mentioning that, for ($\chi < \chi_c < 0$), the aforesaid equations haven't resulting and the complete

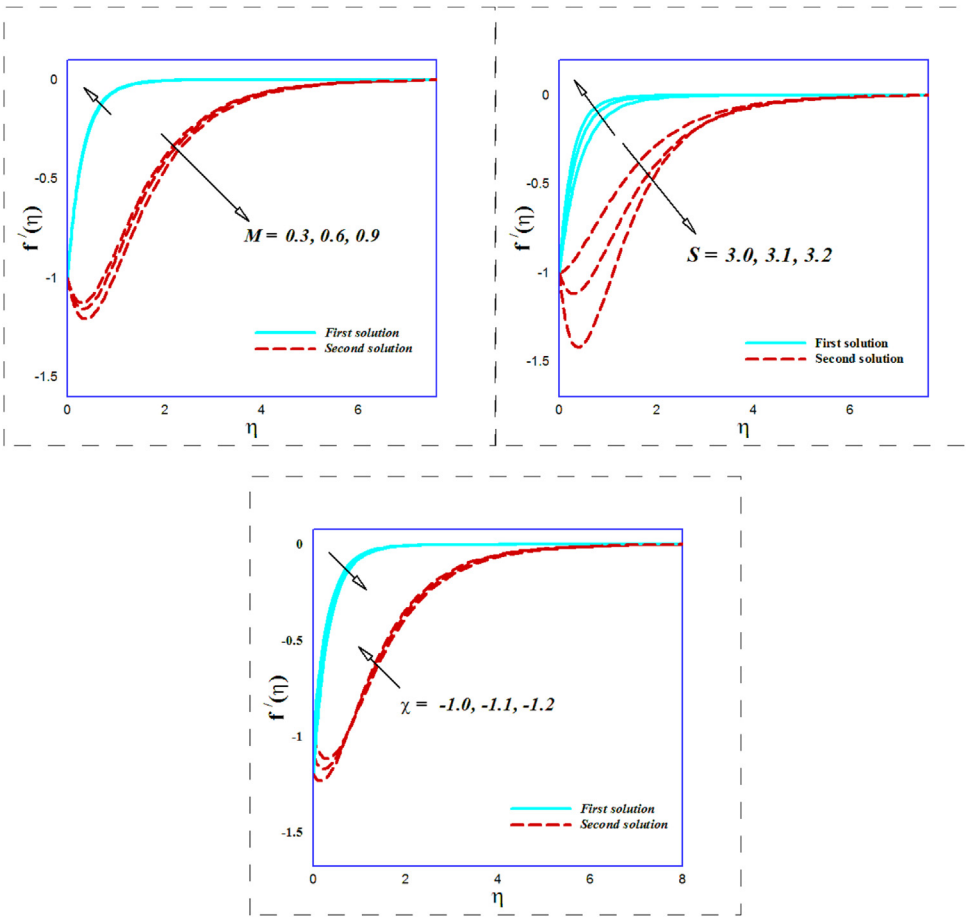

Fig. 5 – (a–c): Profile plots of $f'(\eta)$ for (a) M, (b) S and (c) χ.

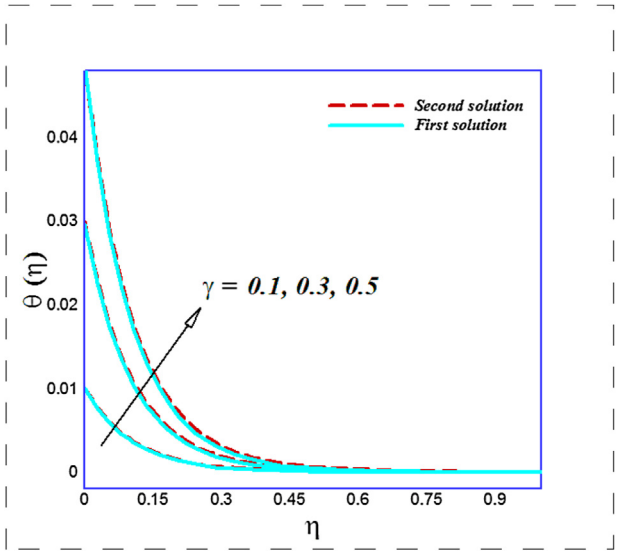

Fig. 6 – Profile plot of $\theta(\eta)$ for γ.

energy, Navier-Stokes and concentration equations ought to be worked out.

To further study the flow dynamics, the variation against suction parameter S of $Af''(0) - [-f''(0)]^n$ and $-\theta'(0)$ for assorted values of material parameter A is illustrated in Fig. 3(a and b). The results in Fig. 3(a and b) explain that the uniqueness and existence of solution also depend on the suction parameter S. It is also seen, that as the material parameter A

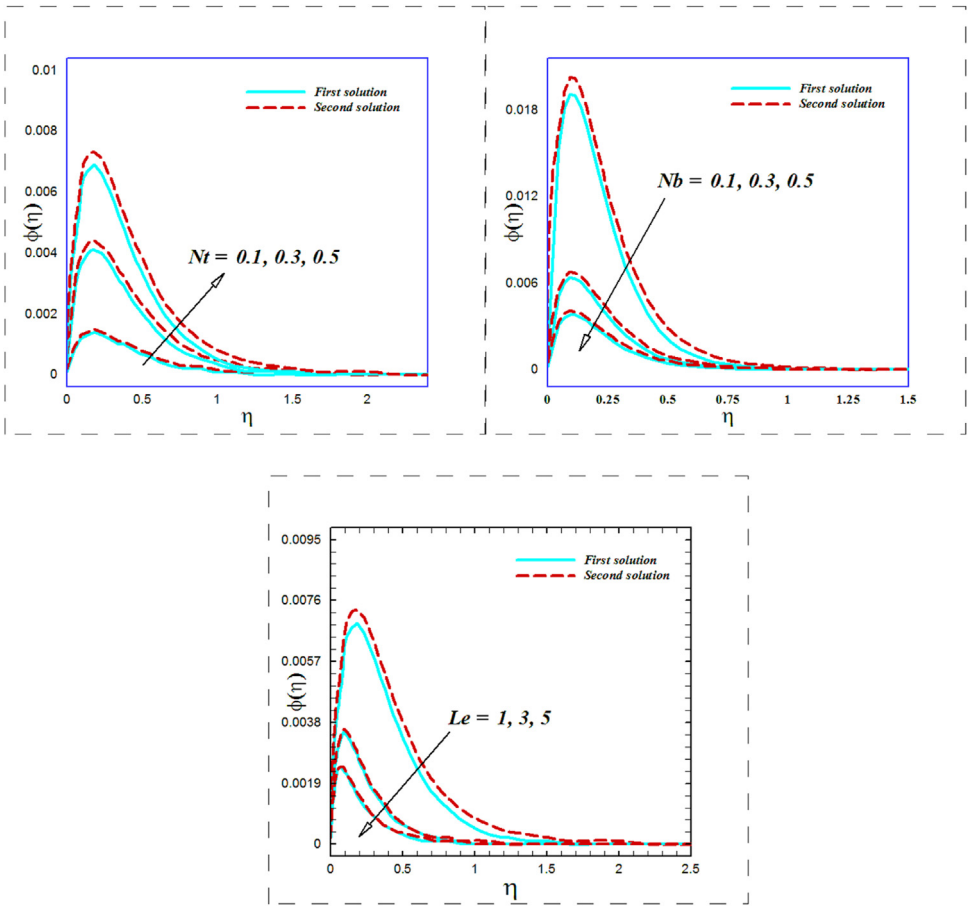

Fig. 7 – (a–c) Profiles plots of $\phi(\eta)$ for (a) Nt, (b) *Nb* and (c) *Le*.

rises, both the first and second solutions of $Af''(0) - [-f''(0)]^n$ and $-\theta'(0)$ bifurcate out to a single solution at the critical point $S = S_c$. Moreover, the range of suction parameter S for which the multiple solutions exist also increases. According to our calculations, it is clear from Fig. 3(a) that the skin friction coefficient decreases as the material parameter increases for both the solutions. The curves in Fig. 3(b) demonstrate that the amount of $-\theta'(0)$ is constantly rising for upper branch in a nanoliquid with growing S. However, a conflicting drift is seen, in the case of the lower branch curves.

In flow circumstances over a shrinking surface, the dual solutions of $Af''(0) - [-f''(0)]^n$ for a variation of material parameter A are portrayed in Fig. 4(a and b). Our results suggest that the multiple solutions are attained for shrinking parameter $\chi \geq \chi_c$ and no solutions are possible for ($\chi \leq \chi_c < 0$). This means that the surface boundary layer separates at a critical value χ_c beyond which the approximation of the boundary layer is not valid. For the first solution, it is also noticed in Fig. 4(a). In Fig. 4(a), the skin friction coefficient depicts a decreasing behavior for increasing values of A. However, a reverse trend is observed for the second solution. In addition, an enhancement in the local Nusselt number $-\theta'(0)$ which symbolizes the heat transfer rate is seen with larger values of material parameter for first solution and opposite is observed for the second solution.

6.2. *Variations in velocity, temperature and nanoparticles concentration*

The velocity profile $f'(\eta)$ for distinct values of magnetic parameter M for the shrinking case $\chi = -1$ is presented in Fig. 5(a). In this Figure, it is perceived that all profiles of velocity consist of two solution branches i.e. upper and lower branch solutions. The dual profiles that an enhancement in magnetic parameter M results in a higher nanofluid velocity for the first solution whilst it shows a decreasing trend in the second solution. It is also worth mentioning that an opposite effect can be observed for the momentum boundary layer thickness. Physically, when a magnetic number is pertained normal to the surface, a ponder motive force proceeds in the uphill direction to enhance the flow and increases the velocity of nanoliquid. Fig. 5(b) indicates the dual profiles of velocity $f'(\eta)$ for varying values of S with the boundary layer regime. The nanoliquid velocity and corresponding boundary layer thickness shrinks with greater suction parameter in first solution, while a quite opposite trend is seen in the second solution as depicted in this Fig. Moreover, the momentum boundary layer rises with growing values of S for the lower branch and numerical solutions are much more suitable in this phenomenon. Physically, due to the suction, the heated liquid is pressed towards the surface where the forces can proceed to improve the nanoliquid due to elevated control of the viscosity. In Fig. 5(c), the impact of

shrinking parameter χ on the nanoliquid velocity is plotted by keeping the other parameter fixed. This Figure proves that the wide field boundary conditions (12) are satisfied asymptotically, which underpins the numerical outcomes acquired for the bvp (7)-(9). As demonstrated through this Figure, that $\eta = 8$ is large enough for the velocity profiles to vanish asymptotically. In addition, we observe that the boundary layer grows to be thicker and thicker for the upper branch as compared to a lower branch solution. Further, Fig. 5(c) indicates that a larger value of shrinking parameter communicates to a higher velocity for the upper solution. Whilst, in the case of lower branch solution, dual trend is noted. It is apparent that near the solid boundary velocity decreases with decreasing values of shrinking parameter and after a certain distance from boundary its start increasing. For first solution, the fluid velocity is comparatively higher than the second solution.

Fig. 6 portrays the variation of temperature profiles $\theta(\eta)$ against η for the distinct values of the Biot constraint γ with fixed values of the other constraints. This Figure confirms the existence of dual temperature profiles for the shrinking sheet. It is seen that temperature at a point accelerates with higher the Biot number for both the solutions. Further, the associated thermal boundary layer thickness enhances. Physically, the heat transfer rate enhances in convective heat transfer phenomenon. Thus, an additional heat is transmuted from the heated surface to the cooled surface of the nanofluid; the temperature augments which transports heat further from the sheet to the liquid. Thus, the temperature of nanoliquid increases for greater γ. The impacts of thermophoresis parameter *Nt*, Brownian motion parameter *Nb* and the Lewis number *Le* on the nanoparticles concentration profiles $\phi(\eta)$ for fixed values of other parameters are elucidated in Fig. 7(a–c), respectively. Fig. 7(a) shows that the nanoparticles concentration augments due to *Nt* in the first and the second solutions. This is due to the fact that the thermophoresis larger influence proceeds to carry the nanomaterials close to the warm surface on the way to cold liquid at the ambient, and therefore, bigger penetration intensity is delivered. Fig. 7(b) depicts that the nanoparticle concentration declines due augmenting *Nb* in the both solutions. Physically, *Nb* has direct contact with the coefficient of Brownian diffusion. Greater *Nb* has a greater coefficient of Brownian diffusion, which declines the nanoparticle concentration. We can observe in Fig. 7(c) that nanoparticles volume fraction over and above the associated boundary layer thickness reduces with higher Lewis numbers for both lower and upper branch solutions. Physically, this occurs due to a reduction in diffusivity of mass or the Brownian motion of the nanomaterial.

7. Main findings

In the given study, we have scrutinized numerically the MHD flow and heat transfer to a Sisko nanofluid at the surface by considering the convective boundary condition. The governing system of PDE's was transmuted to nonlinear ODE's by utilizing suitable non-dimensional variables. The main efforts of this article were to achieve the existence and multiplicity (duality) of numerical solutions for some pertinent parameters. The impacts of several constraints on nanofluids velocity, concentration and temperature along with Nusselt number and skin-friction coefficient were examined in detail. We found that the multiple solutions were survived for shrinking parameter in a specific domain where its solution boosts up by the greater parameter of mass suction. It is mentioned in the graphical results that the critical values of the suction were raised with an increment in the material parameter. Furthermore, with a higher suction parameter, the local skin friction for the first solution was found to be maximum whilst minimum for the second solution. However, the local Nusselt number for both solutions were depicted a reducing trend with rising values of material parameter.

Conflict of interest

The authors declare no conflicts of interest.

Acknowledgment

The authors are grateful to the Deanship of Scientific Research, King Saud University for funding through Vice Deanship of Scientific Research Chairs.

REFERENCES

[1] Xuan Y, Roetzel W. Conceptions for heat transfer correlation of nanofluids. Int J Heat Mass Transfer 2000;43(19):3701–7.
[2] Amiri A, Shanebedi M, Chew B, Kazi S, Solangi K. Toward improved engine performance with crumpled nitrogen-doped graphene based water-ethylene glycol coolant. Chem Eng J 2016;289:583–95.
[3] Choi SUS. Enhancing thermal conductivity of fluids with nanoparticles. Develop Appl. Non- New Flows 1995;231:99–105.
[4] Eastman JA, Choi SUS, Li S, Yu W, Thompson LJ. Anomalously increased effective thermal conductivities of ethylene glycol-base nanofluids containing copper nanoparticles. Appl Phys Lett 2011;78:718–20.
[5] Buongiorno J. Convective transport in nanofluids. ASME J Heat Transfer 2006;128:240–50.
[6] Tiwari RJ, Das MK. Heat transfer augmentation in a two sided lid driven differentially heated square cavity utilizing nanofluids. Int J Heat Mass Transfer 2007;50:2002–18.
[7] Kuznetsov AV, Nield DA. Natural convective boundary-layer flow of a nanofluid past a vertical plate. Int J Therm Sci 2010;49(2):243–7.
[8] Rashidi MM, Abelman S, Mehr NF. Entropy generation in steady MHD flow due to a rotating disk in a nanofluid. Int J Heat Mass Transf 2013;62:515–25.
[9] Sheikholeslami M, Abelman S, Ganji DD. Numerical simulation of MHD nanofluid flow and heat transfer considering viscous dissipation. Int J Heat Mass Transfer 2014;79:212–22.
[10] Khan M, Hashim, Hafeez A. A review on slip-flow and heat transfer performance of nanofluids from a permeable shrinking surface with thermal radiation: dual solutions. Chem Eng J 2017;173:1–11.
[11] Rocha JRS, de Souza EEB, Marcondes F, de Castro JA. Modeling and computational simulation of fluid flow, heat transfer and inclusions trajectories in a tundish of a steel continuous casting machine. J Mat Res Tech 2019;8(5):4209–20.

[12] Khan U, Zaib A, Khan I, Nisar KS. Activation energy on MHD flow of titanium alloy (Ti_6Al_4V) nanoparticle along with a cross flow and streamwise direction with binary chemical reaction and non-linear radiation: dual solutions. J Mat Res Tech 2020;9(1):188–99.
[13] Ahmed Z, Nadeem S, Saleem S, Ellahi R. Numerical study of unsteady flow and heat transfer CNT-based MHD nanofluid with variable viscosity over a permeable shrinking surface. Int J Num Meth Heat Fluid Flow 2019;29(12):4607–23.
[14] Sheikholeslami M. New computational approach for exergy and entropy analysis of nanofluid under the impact of Lorentz force through a porous media. Comp Meth Appl Mech Eng 2019;344:319–33.
[15] Ellahi R, Sait SM, Shehzad N, Ayaz Z. A hybrid investigation on numerical and analytical solutions of electro-magnetohydrodynamics flow of nanofluid through porous media with entropy generation. Int J Num Meth Heat Fluid Flow 2019;30(2):834–54.
[16] Sheikholeslami M, Haq RU, Shafee A, Li Z. Heat transfer behavior of nanoparticle enhanced PCM solidification through an enclosure with V shaped fins. Int J Heat Mass Transf 2019;130:1322–42.
[17] Ellahi R, Sait SM, Shehzad N, Mobin N. Numerical simulation and mathematical modeling of electroosmotic Couette-Poiseuille flow of MHD power-law nanofluid with entropy generation. Symmetry 2019;11(8):1038.
[18] Riaz A, Bhatti MM, Ellahi R, Zeeshan A, Sait SM. Mathematical analysis on an asymmetrical wavy motion of blood under the influence entropy generation with convective boundary conditions. Symmetry 2020;2(1):102.
[19] Sarafraz MM, Pourmehran O, Yang B, Arjomandi M, Ellahi R. Pool boiling heat transfer characteristics of iron oxide nano-suspension under constant magnetic field. Int J Thermal Sci 2020;147:106131.
[20] Ellahi R, Hussain F, Abbas SA, Sarafraz MM, Goodarzi M, Shadloo MS. Study of two-phase Newtonian nanofluid flow hybrid with hafnium particles under the effects of slip. Invention 2020;5(1):6.
[21] Bird RB, Curtiss CF, Armstrong RC, Hassager O. Dynamics of polymeric liquids. New York: Wiley; 1987.
[22] Harris J. Rheology and non-newtonian flow. New York: Longman; 1977.
[23] Sisko AW. The flow of lubricating greases. Ind Eng Chem Res 1958;50(12):1789–92.
[24] Wanga Y, Hayat T, Ali N, Oberlack M. Magnetohydrodynamic peristaltic motion of a Sisko fluid in a symmetric or asymmetric channel. Physica A: Stat Mech Appl 2008;387:347–62.
[25] Abelman S, Hayat T, Momoniat E. On the Rayleigh problem for a Sisko fluid in a rotating frame. Appl Math Comput 2009;215(7):2515–20.
[26] Khan M, Munawar S, Abbasbandy S. Steady flow and heat transfer of a Sisko fluid in annular pipe. Int J Heat Mass Transfer 2010;53:1290–7.
[27] Khan M, Shahzad A. On boundary layer flow of Sisko fluid over stretching sheet. Quaestiones Math 2013;3:137–51.
[28] Khan M, Malik R. Forced convective heat transfer to Sisko nanofluid past a stretching cylinder in the presence of variable thermal conductivity. J Mol Liq 2016;218:1–7.
[29] Hayat T, Ullah I, Alsaedi A, Waqas M, Ahmad B. Three-dimensional mixed convection flow of Sisko nanoliquid. Int J Mech Sci 2017;133:273–82.
[30] Farooq S, Hayat T, Alsaedi A, Ahmad B. Numerically framing the features of second order velocity slip in mixed convective flow of Sisko nanomaterial considering gyrotactic microorganisms. Int J Heat Mass Transfer 2017;112:521–32.
[31] Siddappa B, Abel S. Non-Newtonian flow past a stretching plate. ZAMP 1985;36:890–2.
[32] Ibrahim W, Shankar B. MHD boundary layer flow and heat transfer of a nanofluid past a permeable stretching sheet with velocity, thermal and solutal slip boundary conditions. J Comput Fluids 2013;75:1–10.
[33] Malvandi A, Ganji DD. Magnetohydrodynamic mixed convective flow of Al_2O_3-water nanofluid inside a vertical microtube. J Magn Magn Mater 2014;369:132–41.
[34] Sheikholeslami M, Bandpy MG, Ellahi R, Zeeshan A. Simulation of MHD CuO-water nanofluid flow and convective heat transfer considering Lorentz forces. J Magn Magn Mater 2014;369:69–80.
[35] Aly EH, Ebaid A. Exact analysis for the effect of heat transfer on MHD and radiation Marangoni boundary layer nanofluid flow past a surface embedded in a porous medium. J Mol Liq 2016;215:625–39.
[36] Mabood F, Khan WA, Ismail AIMd. MHD stagnation point flow and heat transfer impinging on stretching sheet with chemical reaction and transpiration. Chem Eng J 2015;273:430–7.
[37] Sandeep N, Reddy MG. Heat transfer of nonlinear radiative magnetohydrodynamic Cu-water nanofluid flow over two different geometries. J Mol Liq 2017;225:87–94.
[38] Ibrahim W. Magnetohydrodynamic (MHD) boundary layer stagnation point flow and heat transfer of a nanofluid past a stretching sheet with melting. Propul Power Res 2017;6(3):214–22.
[39] Kuznetsov AV, Nield DA. Natural convective boundary-layer flow of a nanofluid past a vertical plate. Int J Therm Sci 2010;49:243–7.
[40] Shampine LF, Gladwell I, Thompson S. Solving ODEs with MATLAB. 1st ed. Cambridge: Cambridge University Press; 2003.
[41] Khan M, Malik R, Munir A, Shahzad A. MHD flow and heat transfer of Sisko fluid over a radially stretching sheet with convective boundary conditions. J Braz Soc Mech Sci Eng 2016;38:1279–89.
[42] Miklavčič M, Wang CY. Viscous flow due a shrinking sheet. Q Appl Math 2006;64:283–90.
[43] Fang TG, Zhang J, Yao SS. Viscous flow over an unsteady shrinking sheet with mass transfer. Chinese Lett 2009;26:014703.